CHAPTER 1

INTRODUCTION

Microwave photonics is a multidisciplinary field that encompasses optical, microwave, and electrical engineering. The microwave photonics field must therefore span frequencies of below 1 kHz in the radio-frequency (RF) domain to frequencies of hundreds of terahertz associated with the optical domain. The field originated from the need to solve increasingly complex engineering problems when radio engineers ventured outside their discipline to the optical domain in search of new capabilities. Generally, the field is applied in nature stemming from its roots and driven by present-day system needs. However, many basic research areas are associated with the underlying component technologies.

Although the field of microwave photonics was not formalized internationally until the late 1980s and the early 1990s (Berceli and Herczfeld, 2010), its history spans more than a few decades. The use of RF for telegraph communications in the early to mid-1800s gave birth to the need for radio engineers. However, it was not until the expanded development of radar during World War II (Page 1962) to search for aircraft electronically did the need for those with analog or radio engineering skills increase dramatically. Nearly as quickly as

Fundamentals of Microwave Photonics, First Edition.
Vincent J. Urick Jr, Jason D. McKinney, and Keith J. Williams.

radar was established as a useful tool to aid in detection, radar countermeasures were developed to confuse and deny the radar operators effective use of their new tools. Countermeasures necessitate radar redesign in order to render countermeasures ineffective. This iterative countermeasure/counter-countermeasure battle continues today and will so long into the future as the radar designer is constantly trying to "see and not be seen" (Fuller 1990). The use of higher frequencies and the desire to delay those frequencies created a need for low loss delay lines. The early promise of microwave photonics technologies for low loss long delay lines is closely linked to this radar and electronic countermeasure battle.

Today's society makes abundant use of the electromagnetic spectrum for communication. Radio and television broadcasts, cell phones, satellite communications, push-to-talk radios, and many other techniques have been developed to facilitate communication between two or more parties. These systems make use of RF signal transmission and processing within the devices. Due to the expansion of microelectronic circuits and their size/power/speed advantages, many of these systems have moved from strictly analog systems to mixed-signal implementations. In these systems, analog signals are digitized, processed, and/or transported in digital form before being converted back to continuous waveforms for use in the analog world. Although modern RF systems increasingly use digital signal processing (DSP), analog fiber optic links offer the radio engineer significant and useful tools in the design of these systems. The ability to process a signal in the analog domain can simplify overall system design, especially in wide bandwidth systems, where bandwidth demands are difficult to achieve with DSP. However, the analog system engineer should use the best analog tools along with the features that DSP can provide to make the most efficient and powerful system possible.

In its most basic form, an analog photonic link is a delay line containing an electrical-to-optical (E/O) converter to transform the RF signal into the optical domain, an optical transmission medium, and an optical-to-electrical (O/E) converter. Figure 1.1 illustrates a functional block diagram for a multichannel fiber optic link. One or more RF inputs are converted into the optical domain by E/O converters. Once the RF signal has been transformed into the optical domain, it can be delayed in time with optical fiber, processed, and delivered to one or more O/E converters where the optical signals are demodulated back into electrical RF signals. The processing elements can take many forms, including switching, routing, filtering, frequency translation, and

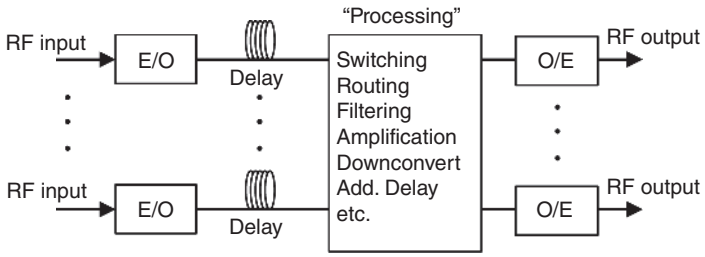

Figure 1.1. Basic block diagram of an array of fiber optic links.

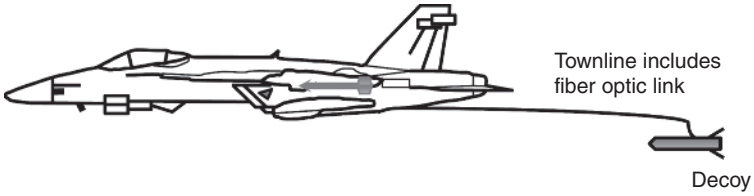

Figure 1.2. A depiction of an RF towed decoy from an F/A 18.

amplification, to name a few. The performance of various forms of such analog photonic links will be treated throughout the middle chapters.

Fiber optic links have proved to be advantageous over their electronic (coaxial cable) counterparts for a number of applications. One of the early military applications was the use of a fiber optic link in an airborne towed decoy as shown in Figure 1.2, the ALE-55. The concept of a towed RF transmitter from an aircraft to distract an RF-guided missile away from its intended target has existed since, at least, the 1960s (Norman and Meullen, 1964), with fiber optic versions appearing later (Toman 1989). In early designs, a receiving antenna on the decoy detected a threat, amplified, and then re-transmitted a higher power return signal. However, due to the size limitations necessitated by aerodynamics of the decoy, only a limited amount of signal processing can be performed on the decoy itself. The use of a fiber optic cable to connect the airplane and the decoy makes it possible to use sophisticated signal processors onboard the aircraft, remoting processed signals to the decoy where amplification and transmission occur. This allows the decoy to be used in a multiphase approach for defeating a threat missile including suppressing the radar's ability to track the aircraft, deceiving the radar with jamming techniques, and seducing the missile away from the aircraft by presenting a more attractive target. Fiber optics minimizes the size of

the decoy and reduces the tension on the decoy towline, allowing it to be useful on a wider variety of aircraft.

One of the first widespread commercial uses of analog fiber optic links was in hybrid fiber-coaxial (HFC) systems for cable television signal distribution (Chiddix et al. 1990). HFC solutions offered cable system operators the ability to increase the number and quality of video signals delivered to the home and to provide upstream broadband data services at low cost with high reliability. HFC systems transformed the role of the cable industry from being strictly a provider of video to a viable competitor in the local access market, traditionally served by the telephone system. Combined with the expansion of the Internet, this has helped to shape the competitive broadband information infrastructure as it exists today. By the mid-1990s, HFC systems were capable of delivering over 100 channels of amplitude-modulated vestigial-sideband (AM-VSB) video distances of over 20 km with a variety of optical link designs. The key to this success was the ability to deliver video signals optically having high carrier-to-noise ratios (CNR) and low composite second-order (CSO) and composite triple-beat (CTB) distortion levels. Significant early work on improving the linearity of analog optical links was performed for this application, including work on linearizing external modulation (Nazarathy et al. 1993) and study of crosstalk due to optical fiber nonlinearities (Phillips and Ott 1999). A significant portion of this book is devoted to sources of nonlinearity in analog optical links. Almost as quickly as HFC changed the cable and telephone industry, conversion from AM-VSB video distribution to compressed digital video (CDV) began. Although the conversion was slow due to the cost of replacing an entrenched and expensive infrastructure, CDV has now displaced much of the AM-VSB video distribution technologies. As with the legacy AM-VSB signals, fiber optic links remain the transmission medium of choice for such modern telecommunication systems.

In radio astronomy, large antennas are used to detect RF emissions from space. Microwave engineering plays a crucial role in radio astronomy, with analog fiber optic links being used in modern systems (Webber and Pospieszalski 2002). The Greenbank Telescope (GBT), located in West Virginia and operating from 0.1 to 115 GHz, is the world's largest fully steerable single antenna (Lockman 1998, Prestage et al. 2009). The 100-m-diameter parabolic antenna is used to enhance scientific understanding in areas such as the detection of gravitational waves (through precision pulsar timing); the formation of stars, galaxies, and galaxy clusters; and the composition of planets. The antenna is used

for the detection of atomic and molecular emission lines spanning from high red-shift situations (emissions near black holes) to those where the measurement of weak, spatially extended spectral lines can be used to detect new organic molecules in space. The GBT uses an analog fiber optic link for remoting signals to a processing laboratory (White 2000). For higher spatial resolution, smaller dish antennas can be used in a phased-array configuration to take advantage of long baselines to measure small phase changes. Such an array was inaugurated in 2013 in the mountains of Chile (Testi and Walsh 2013), a portion of which is shown in Figure 1.3. Fiber optic links to remote the millimeter wave signals have shown potential utility in large radio astronomy antenna arrays (Payne and Shillue 2002). Because the RF signals originate at astronomical distances and are thus very low power, large antenna systems with very low noise figures are assembled and operated as large phased arrays. Such systems take advantage of the array gain from a large effective aperture and the phase sensitivity of a long baseline. In some systems, as many as 64 12-m dish antennas operating over a 16-km baseline must have their RF signals coherently summed at a central location. Since the frequencies of interest may reach hundreds of gigahertz, relative path differences must be precisely accounted for. This is very challenging, even for fiber optics (Thacker and Shillue 2011), as temperature variations, polarization drift, and chromatic dispersion all lead to length errors requiring active compensation. Additional details on the fiber links for the GBT and ALMA are provided in Chapter 10.

Figure 1.3. The Atacama large millimeter/sub-millimeter array (ALMA) interferometer in Chile. (*Credit:* ALMA (ESO-NAOJ-NRAO), J. Guarda.)

The aforementioned applications are just a few of the many within RF, microwave, or millimeter-wave systems where fiber optic links have proven useful. Microwave photonics provides utility in areas spanning the military, industrial, and academic sectors. Other applications include radio-over-fiber for wireless communications, delivering power to and from antenna feeds for antenna and array calibration, signal routing and true time delay beamforming in arrays, optical signal processing, filtering, waveform synthesis, optoelectronic oscillators for the precision generation of RF signals, optical clocks for precision timing, and RF downconverters and upconverters. The underlying technology and components contained within analog optical links are the subjects of this book, including more detail on applications of the technology in Chapter 10.

1.1 ENABLING TECHNOLOGICAL ADVANCES AND BENEFITS OF FIBER OPTIC LINKS

The frequency range of interest to the field of microwave photonics depends to a large degree on Mother Nature. Figure 1.4 (Liebe 1983) shows the atmospheric attenuation of RF radiation at sea level under different atmospheric conditions. As can be seen, there are

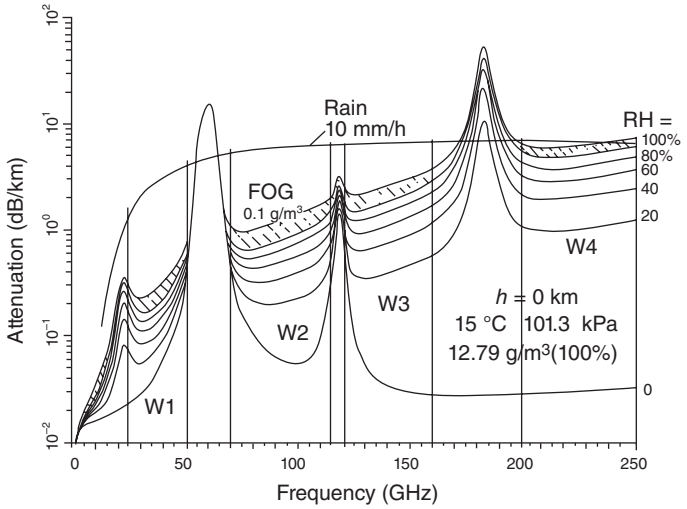

Figure 1.4. Specific atmospheric attenuation at sea level for various levels of relative humidity (RH), including fog and rain. Transmission windows are designated W1–W4 (Liebe 1983).

strong absorption bands near 23, 60, 119, and 182 GHz. Between these frequencies are transmission "windows" with comparatively less loss. Systems using frequencies below 20 GHz have proliferated for ground-based or sea-level applications, with a few systems operating in the second and third windows, centered around 35 and 94 GHz, respectively. Inspection of Figure 1.4 implies that these systems are functioning with an atmospheric attenuation of 0.3 dB/km or less at sea level. At altitudes above 9.2 km, the attenuation decreases in these atmospheric transmission windows to below 0.05 dB/km at frequencies up to 300 GHz (Wiltse 1997). Given that 0.3 dB/km is an acceptable level of attenuation at sea level, it then becomes plausible to consider the use of frequencies up to 300 GHz at high altitudes such as in air-to-air applications. In terms of fractional bandwidth, 300 GHz is only 0.16% of the bandwidth of an optical carrier at 1550 nm (193 THz). This small fractional bandwidth allows many applications to be realized in photonics, including RF signal multiplexing. In addition, many photonic device technologies have been shown to be feasible in the 100–300 GHz range, making the technology suitable throughout this entire frequency range (see Section 10.5). The field of microwave photonics evolved largely due to such application needs. However, before the technology could prosper, several significant breakthroughs were needed, including low loss optical fibers and efficient high bandwidth transducers (E/O and O/E).

Figure 1.5 shows a typical cross-section and index profile for a step index optical fiber. A high index glass core having index of refraction n_1 and diameter d_1 is surrounded by a slightly lower index glass cladding

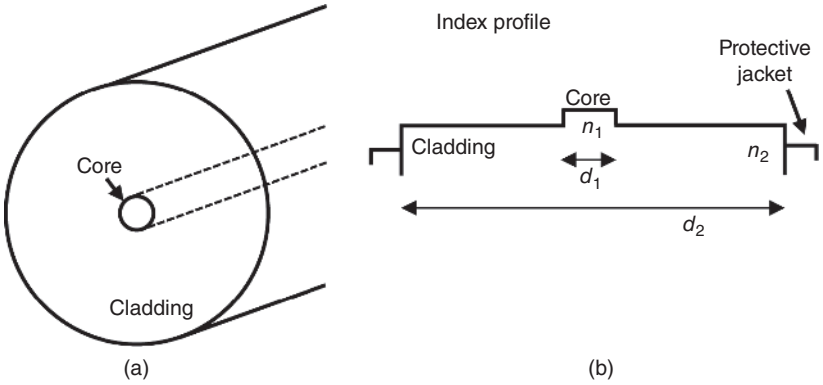

Figure 1.5. (a) Depiction of single mode fiber core and cladding regions with index profile (b) for a step index waveguide design.

having index n_2 and diameter d_2. The cladding is sufficiently thick such that the evanescent electric field of the propagating mode(s) exponentially decays in this region. The cladding glass is usually coated with a lower index polymer for environmental protection. Typical core and cladding diameters are from 8 to 50 μm and from 60 to 125 μm, respectively. The core–cladding index difference and the diameter of the core determine how many propagating modes the fiber waveguide can support for a particular wavelength.

Maxwell's equations describe the propagation of waves within the dielectric waveguide of an optical fiber. From a solution to the wave equations, a normalized frequency or V-number for the fiber can be defined as

$$V = \frac{\pi d_1}{\lambda}\sqrt{(n_1^2 - n_2^2)}, \tag{1.1}$$

where λ is the wavelength. For typical optical fibers, the normalized index difference, $\Delta = (n_1 - n_2)/n_1$, is usually $\ll 1$, and Equation (1.1) reduces to

$$V = \frac{\pi d_1}{\lambda} n_1 \sqrt{2\Delta} = \frac{\pi d_1}{\lambda}\mathrm{NA}, \tag{1.2}$$

where NA is the numerical aperture of the fiber. In ray optics, NA = $n_0 \sin(\theta)$, where θ is the acceptance half-angle, and n_0 is the index of the material in front of the fiber interface ($n_0 = 1$ for air). The NA is a measure of the light-gathering capacity of a fiber whereby light impinging on the fiber at an angle greater than θ relative to the propagation axis does not excite a guided mode. One can show that for all values of V up to the first zero of the Bessel function J_0 such that $J_0(V) = 0$ (see Appendix VI) that the waveguide can only support the lowest order hybrid mode, HE11 (Ramo et al. 1994). Thus, for $V < 2.405$, the waveguide is single mode. When V exceeds 2.405, the waveguide supports higher order modes, and for large V, the number of supported modes can be estimated to be $V^2/2$. A typical single mode fiber at 1550 nm has a core diameter of 10 μm, allowing for an index difference of 0.006 or less to remain single mode. Such small index differences are possible by adding dopant materials such as GeO_2, P_2O_5, or B_2O_3 to pure fused silica glass (SiO_2).

Multimode fibers with larger cores were fabricated earlier than single-mode fiber and typically achieved lower loss due to the higher tolerances to waveguide dimensional imperfections. However, RF photonic links at high frequencies use single-mode fibers almost exclusively to avoid power fading experienced in multimode fibers due to

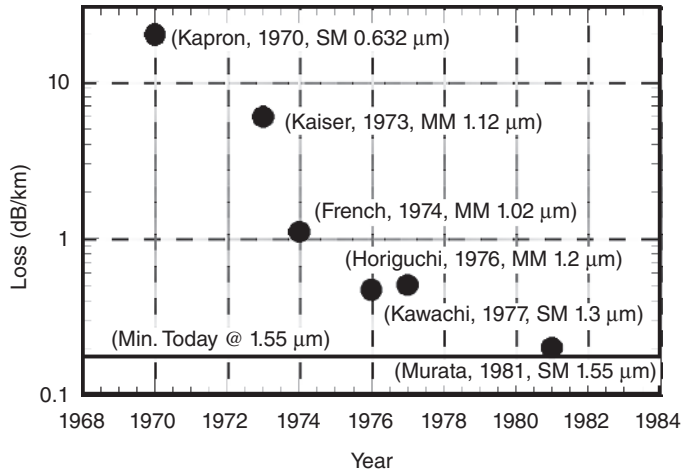

Figure 1.6. Reported losses in optical fiber over time for single-mode (SM) and multimode (MM) fibers at various wavelengths (French et al., 1974;Horiguchi, 1976; Kaiser, 1973; Kapron, 1970; Kawachi, 1977; and Murata and Inagaki, 1981).

modal dispersion. Figure 1.6 shows the progress over time of the optical losses of multimode and single-mode fibers in terms of propagation loss. Fundamentally, the loss is limited by Rayleigh scattering in the fiber, which amounts to a loss of 0.175 dB/km at 1550 nm. As can be seen from Figure 1.6, fiber loss decreased to below 1 dB/km by 1974 and was within 10% of the Rayleigh scattering limit by 1981. It will be demonstrated in later chapters that for many link modulation formats, the RF loss in a microwave photonic link is twice that (in decibels) of the optical loss. Therefore, by 1981, RF delay line propagation loss would have been as low as 0.4 dB/km at 1550-nm wavelength. Since the wavelength dependence of the loss is minimal over a few nanometers bandwidth (hundreds of gigahertz bandwidth at 1550 nm), the RF propagation loss is practically frequency independent.

Low optical fiber loss offered the promise of substantial performance advantages in RF delay lines if the subsequent transducers from E/O and O/E could be developed in the frequency ranges of interest. Initially, the most important frequency range of interest was the region below the first atmospheric absorption feature including frequencies up to 20 GHz (Figure 1.4) where a substantial number of deployed RF systems existed. On the E/O side, the semiconductor laser was an early choice due to the sub-ns photon lifetimes in GaAs (wavelengths up to 860 nm) and InGaAsP (wavelengths up to 1600 nm). Direct modulation of the pump current for these lasers provides a straightforward E/O

mechanism. Demonstrations up to 10 GHz modulation bandwidth were prevalent by the mid-1980s (Su and Lanzisera 1986). The first demonstration of a semiconductor laser to surpass 20 GHz bandwidth was at 1.3 μm, using a buried heterostructure in a bulk material (Olshansky et al. 1987). Research continued in this area to improve differential efficiency (leading to higher E/O conversion efficiency) and to increase bandwidth. It was widely expected that multiple quantum well laser designs would help to improve differential efficiency because of their carrier confinement properties and low carrier densities required for inversion (Okamoto 1987). However, it was not until the high speed carrier transport into and out of the quantum wells was studied and understood (Nagarajan et al. 1992) that the bandwidths of quantum well lasers exceeded those made without quantum confinement. Distributed feedback (DFB) laser designs quickly followed, allowing for single-longitudinal-mode operation. While 20 GHz bandwidth lasers satisfy a large number of RF system applications, semiconductor laser intensity noise near the modulation bandwidth limit peaks, leading to lower signal-to-noise ratios (SNR). This intensity noise (or relative intensity noise—RIN) peak can be mitigated by increasing the modulation bandwidth; DFB lasers achieving 25 GHz bandwidth at 1550 nm (Morton et al. 1992) and over 40 GHz bandwidth (Weisser et al. 1996) have been reported.

On the back end of the link, an O/E converter is required to convert RF modulation impressed on the optical carrier back into an RF signal. The most significant device for this is the p–n junction photodiode incorporating a depleted intrinsic region to reduce capacitance, referred to as a p–i–n photodiode. Early work on high speed photodiodes yielded substantially higher bandwidths than their high speed laser counterparts (Bowers et al. 1985), and photodiodes were generally not the bandwidth-limiting device within the first links. There are design trades for these photodiodes when implemented in bulk surface-illuminated structures (Bowers and Burrus 1987); increasing the depletion region thickness lowers capacitance (increases bandwidth) and improves absorption efficiency but causes carrier transit times to increase (decreasing bandwidth). This tradeoff can be avoided by using waveguide or distributed traveling wave designs that improve both efficiency and bandwidth at the expense of device and packaging complexity.

In addition to low propagation loss, the information bandwidth available and the frequency independence of the loss in fiber are just as

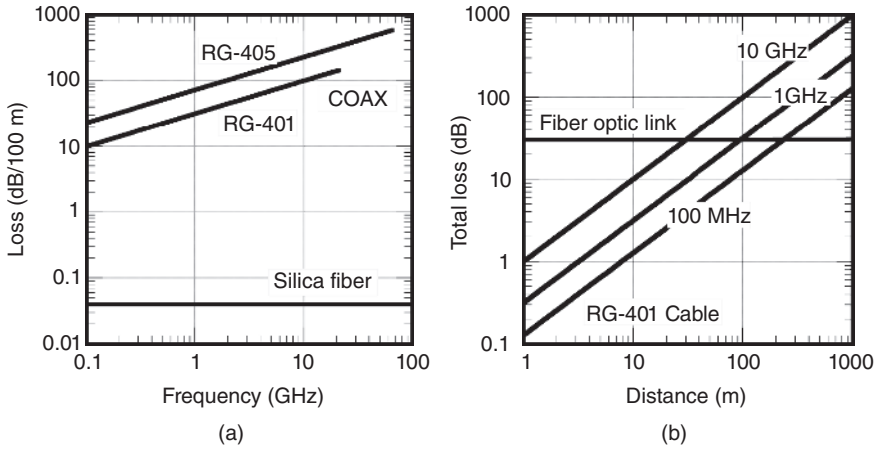

Figure 1.7. Loss as a function of (a) frequency including only propagation loss in the cable for RG-401, RG-405 and silica fiber and (b) propagation distance for RG-401 at three frequencies. In (b), the fiber optic loss includes a 30 dB fixed loss due to E/O and O/E conversion.

important for RF fiber optic links. This is in stark contrast to propagation loss in an RF coaxial cable that tends to have a square root dependency with frequency. As an example, consider Figure 1.7(a) where the propagation losses in two coaxial cables, RG-401 and RG-405, are plotted versus frequency along with the propagation losses of optical fiber. In general, larger diameter cables such as RG-401 tend to have lower loss but also have a lower cutoff frequency for the waveguide to remain single mode. Note how the coaxial cable loss increases by one decade for every two decades in frequency, characteristic of losses that have a square root dependency with frequency. Note also that the propagation losses in coaxial cable are two or three orders of magnitude higher than those of optical fiber. This reason by itself has led the push for the further development of microwave photonics technology through the present day.

When E/O and O/E transducer losses are included with the propagation loss in the comparison between coaxial cable and fiber, the differences are not quite as pronounced as Figure 1.7(a) might suggest. The total loss in a fiber optic link and the propagation loss in RG-401 at three different frequencies are plotted in Figure 1.7(b) as a function of distance. Included in the fiber optic link loss is a 30-dB transducer loss due to the E/O and O/E conversion losses. Because of the exceptionally low propagation loss, there will always

be a length for which the fiber optic link will outperform coaxial cable from a loss perspective. This crossover distance tends to be higher at lower frequencies, but distances between tens of meters to a few hundred meters are typical. If loss were the only factor, long distance links would always use fiber; however, factors other than loss also contribute to the decision matrix. Cost, noise performance, phase stability, size, immunity to electromagnetic interference (EMI), and other factors can all play a role. These additional considerations can tip the scales toward fiber optics even for very short links. For example, the relative phase change after propagating an optical fiber is compared to that for a coaxial cable using normalized units of parts per million (ppm) in Figure 1.8. Coaxial cable comprises many different materials including solid and stranded metals, different metal types, and various dielectric materials, all having their own coefficients of thermal expansion. This causes the group velocity of coaxial cable to be a complicated function of temperature. In contrast, optical fiber is primarily made from fused silica. Changes in the propagation delays with temperature are due to the temperature dependencies in both the physical waveguide length and in the index of refraction (also see Section 5.3). Uncoated fiber, if it is not mechanically attached to another material with a large thermal expansion coefficient, has an 8 ppm change in delay per unit length per degree of temperature (Hartog et al. 1979). This includes both the material and waveguide dimensional temperature dependencies. The length fluctuation is both very low and very predictable over a wide temperature range, so long as the temperature dependencies associated with fiber coating or cabling

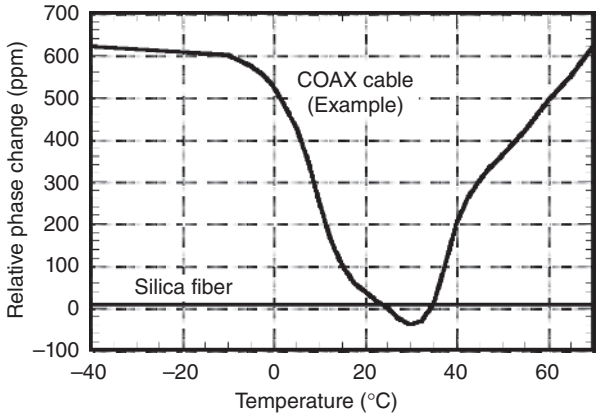

Figure 1.8. Relative phase change versus temperature for a coaxial cable and for optical fiber.

techniques are minimized. This property can be very advantageous in systems where phase stability or phase predictability in the link is a requirement.

Other often-cited advantages associated with fiber optic links include (i) the available bandwidth of over 10,000 GHz, (ii) the reduced size of cable, where sub-millimeter diameters of optical fibers compare to 3–10 mm or larger diameter coaxial cables, (iii) the associated reduction in weight if one can minimize the protective materials needed for cabling, (iv) nonconductive or nonmetallic elements, making the fiber useful in cases where electrical isolation between transmitter and receiver is needed, (v) environmental advantages such as being submersible in fluids, liquid nitrogen, and so on, and (vi) being impervious to corrosion. Analog fiber optic links afford additional less-obvious advantages that are difficult or impossible to achieve electrically. These features include the ability to achieve variable true time delay or RF signal multiplexing. For the latter, the advantages of bundling small fibers into close proximity within a single cable allows for a reduction in the temperature dependence between fiber links (Roman et al. 1998a). This allows for better phase tracking among multiple fiber links, which may be used in phased array applications. As an alternative to multiple fibers, the exceptionally wide bandwidth in the fiber can be used to multiplex numerous RF signals onto one fiber link using different optical carriers. Such multiplexed links and the associated nonlinearities were first studied as a means to distribute cable television channels (Phillips and Ott 1999) and later for higher frequency microwave signals from antenna arrays (Campillo et al. 2003). Many of these advantages and their impact on link performance are discussed throughout this text.

1.2 ANALOG VERSUS DIGITAL FIBER OPTIC LINKS

The RF photonics technology that exists today would not be possible if it were not for the use of fiber optics in digital communication systems. The use of optical fiber to transport digital bits of information across the globe has fundamentally changed the way the world communicates. The Internet and an associated thirst for bandwidth have necessitated the rapid development and deployment of multichannel fiber optic data links to squeeze every last bit of information capacity from a single strand of fiber. An additional benefit of the widespread use of optical fiber for telecommunications is the availability of a vast array of components, many of which can be leveraged for microwave photonics.

Economies of scale and the commoditization of many of these devices have reduced the cost of analog links, except in those cases where specialized components are needed that have no dual use in digital systems.

The differences between analog and digital optical communication links can be substantial. In the digital domain, ones and zeroes can be encoded into optical links as groups of photons (an optical pulse) or the absence of photons. Whether the one or the zero is associated to the actual pulse is not relevant. Noise and timing uncertainty can corrupt the signal during modulation, propagation, and/or detection. So long as the noise and timing uncertainty are small, an integrator can accurately distinguish a pulse from the absence of a pulse using a threshold-like decision in a given time window. In early optical communication links, electrical regenerators periodically removed the noise and timing uncertainty and regenerated the information, thus allowing for propagation over very long distances. In contrast, analog systems must account for the presence of or minimize the effects of this noise and timing uncertainty. In many digital systems today, electronic regenerators are minimized or avoided altogether due to cost implications. Therefore, many long-haul digital communication links are essentially analog, in the sense that the quantization occurs at the link output after transmission.

To expand on this point, Figure 1.9 shows a block diagram of a typical long-haul digital communications link. A digital signal (sequence of ones and zeroes) is input to an E/O converter. Since the attenuation over the entire length of propagation would not allow for detection with a low error rate, the signal must be amplified periodically by several optical amplifiers, typically erbium-doped fiber amplifiers (EDFAs). At the end of the link, O/E conversion returns the waveform to the electrical domain for processing with electronics. The input digital waveform (shown on the middle left) is a series of ones and zeroes denoted by two voltage states. This is simply a baseband RF waveform and can be represented by its Fourier transform or equivalently its spectral content as shown in the lower left plot. A periodic pseudorandom non-return-to-zero (NRZ) waveform has a spectral content of individual lines having an amplitude envelope of a $\sin c^2(f)$ function with frequency spacing that is the inverse of the pattern length (Redd and Lyon 2004). Also shown in Figure 1.9 are noise levels. At the output of the link, noise is added due to the amplification stages. In this illustration, the fundamental clock frequency associated with the bit rate has been enhanced as might occur when a small level of chromatic dispersion in the link causes pulse broadening. Such a “digital” link

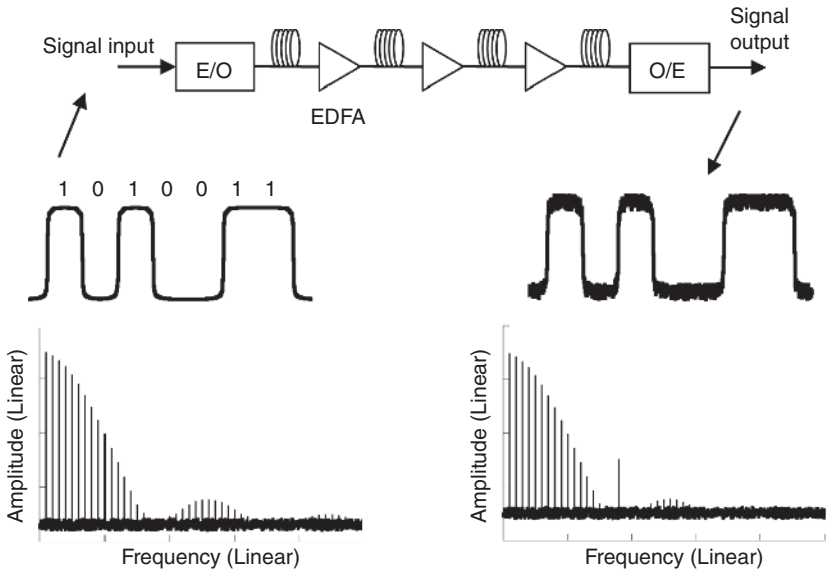

Figure 1.9. Depiction of a long-haul fiber optic link intended to transport digital waveforms. The input digital waveforms with their characteristic baseband RF spectrums are shown both at the input and at the output. The output spectrum depicts a higher noise level due to periodic amplification and distortion leading to the rise of the clock frequency component.

can be viewed as an analog optical system that transports a multitude of RF frequencies from one end to the other. This is only true so long as there are no decision elements involved in the transport as would occur if there were an in-line digital regenerator that detects, retimes, and reshapes the waveform. A current emphasis in digital fiber optic communication systems is to extend the total transmission distance between these electrical regenerations (or repeaters) or even eliminate them altogether to reduce cost and complexity.

Because of the seemingly ever-growing need for bandwidth, optical communications systems have pushed the limits of spectral efficiency within a single optical fiber (Essiambre et al. 2010). Shannon (1949) published a seminal article on the SNR needed to transport a certain number of bits per second in a given unit of bandwidth for a linear information channel, whether that channel is fiber optic, coaxial cable, or otherwise. Shannon's limit can be expressed as

$$C = B \log_2 (\mathrm{SNR} + 1), \tag{1.3}$$

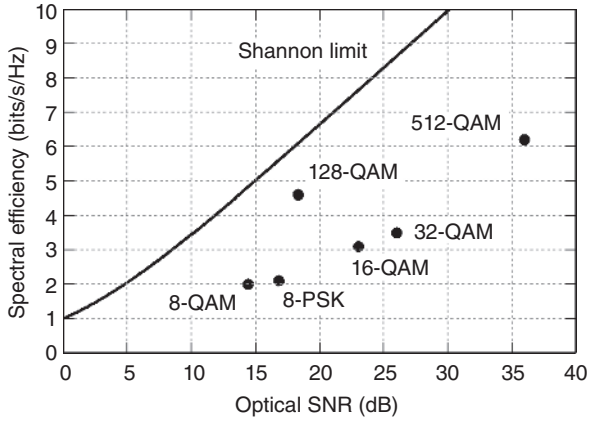

Figure 1.10. Channel capacity as a function of optical signal-to-noise ratio (SNR) according to Equation (1.3). Reported results are also plotted for quadrature-amplitude-modulation (QAM) and phase-shift-keyed (PSK) experiments, showing data for 8-PSK (Zhou et al. 2008), 8-QAM (Zhou et al. 2010), 16-QAM (Winzer et al. 2010), 32-QAM (Takahashi et al. 2010), 128-QAM (Nakazawa 2010) and 512-QAM (Okamoto et al. 2010).

where C is the bit rate in a channel with bandwidth B, and SNR is the output signal-to-noise ratio (linear form, not expressed in dB). The ratio C/B is the channel capacity per unit bandwidth and is denoted as the spectral efficiency in units of bits per second per hertz. Figure 1.10 plots the spectral efficiency given by Equation (1.3) as a function of SNR. Also plotted in Figure 1.10 are several results for various modulation formats. The limiting factor for increasing the information capacity of optical fiber is SNR; however, SNR cannot continue to increase without bound. Since noise cannot be completely eliminated, the signal level must be increased to raise the SNR. At high SNR, fiber nonlinearities limit the attainable spectral efficiency. The nonlinear Shannon limit (Mecozzi and Essiambre 2012, Essiambre et al. 2013) must be employed in this regime, which results in smaller spectral efficiency than predicted by Equation (1.3). It is also important to maximize the output SNR in analog RF systems, as this improves the analog noise figure. Thus, an analog optical RF engineer can leverage work in the optical communications field. In fact, the distinction between lightwave links transporting digital and analog information is becoming blurred. It is not surprising that the performance of many components in the more advanced multilevel digital systems has more stringent performance metrics such as frequency response ripple, laser linewidth, and photodetector amplitude balance, parameters that are typically important in analog links.

With the large and expanding capacity of digital transport and processing systems, it may appear that all analog signals can be digitized immediately and processed in digital form. This is not always possible as discussed in the following section. According to Nyquist (1928), an analog signal can be converted to digital form without deformation as long as the signal is sampled at regular intervals with a minimum of two samples per period of the highest frequency present. To represent the samples in digital form after sampling, the amplitude of the samples must be quantized into discrete levels and to each assigned a digital number. Assigning the amplitude of the sample to one of these discrete levels leads to a quantization noise. This quantization noise is additive to other noise in the signal itself. Let the ratio of the squares of maximum signal voltage to the minimum discernible signal voltage be denoted as a SNR,

$$\text{SNR[dB]} = 20\log\left(V_{\text{max, rms}}/V_{\text{min, rms}}\right). \tag{1.4}$$

If the difference between the quantization levels is uniform (not necessarily a requirement) and comprise 2^n discrete levels, then the SNR reduces to (Walden 1999),

$$\text{SNR[dB]} = 20\log\left(\frac{\sqrt{3}}{\sqrt{2}}2^n\right) = (6.02)n + 1.76. \tag{1.5}$$

Thus, it is often specified that an n-bit analog-to-digital converter (ADC) has a dynamic range of 6.02 dB per effective bit (neglecting the 1.76 dB offset).

Consider a phased-array radar consisting of 1000 receiving elements operating with 10 GHz instantaneous bandwidth. Radars often require 90 dB or more SNR (Roman et al. 1998b), requiring an ADC with 15 bits. Sampling at the Nyquist frequency requires 20 Giga samples per second (Gsps), with each sample being represented by a 15-bit quantization word. The result in this case is an aggregate minimum bit rate of 300 Gb/s per antenna. Assume that an ADC with these specifications is feasible, although this is beyond current technology capabilities (Walden 2008, Khilo et al. 2012). Now, because this is a phased array, the output of all 1000 elements must be processed coherently, and thus the total data rate that must be processed is 300 Tb/s. Although feasible, this is an overwhelming amount of data to manage and process. Analog signal processing or beamforming may always be necessary, as the system requirements for larger dynamic range, instantaneous bandwidth, and array size may increase at a faster rate than the improvements made in digital processing.

1.3 BASIC FIBER OPTIC COMPONENTS

A thorough understanding of analog photonic links and systems cannot be obtained without first understanding the characteristics and performance of the underlying component technologies. A few basic components are introduced in this chapter, so the reader can relate the metrics in the next few chapters back to the basic link configuration block diagram of Figure 1.1. First and foremost, devices that convert electrical signals into the optical domain are required. In the infancy of fiber optics, the diode laser provided this function using direct modulation of the injection current. Figure 1.11 shows a conceptual transfer characteristic for a directly modulated laser. The output power from a laser diode increases rapidly and approximately linearly with injection current above a certain threshold. The threshold current is necessary to cause carrier inversion and to overcome losses in the laser cavity. In either analog or digital modulation, the laser is biased above threshold. An input modulation current causes the intensity of the laser output to vary. In the digital scenario, the laser is nearly turned off for the digital "zero" and to some higher value for the digital "one." This results in nearly 100% modulation depth of the laser diode. For analog links, the

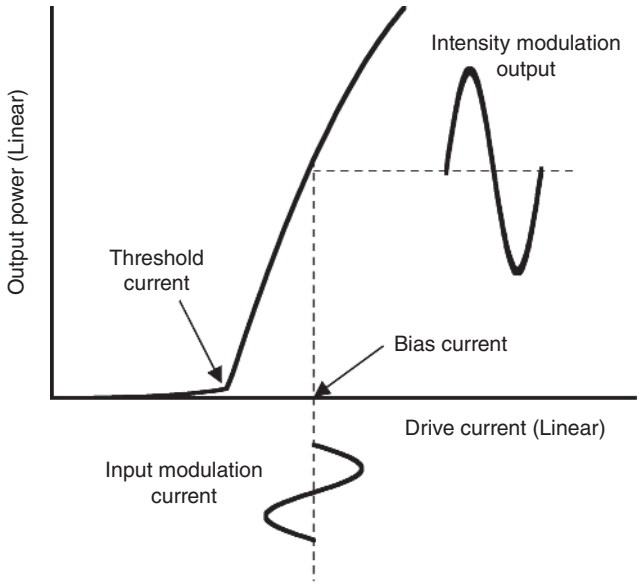

Figure 1.11. Conceptual transfer characteristics of a directly modulated laser diode. The diode is biased with a fixed DC current, and the current is modulated by an RF input signal about this point.

modulation depth varies as the input modulation current amplitude depends on the RF signal level input. To support high dynamic range (a wide range of input RF signal levels), a high bias current is employed to prevent large signals from clipping as the negative swings in signal amplitude push the current down towards the threshold current. A second and often competing issue is the linearity of the current–power curve. As the drive current increases, many diode lasers exhibit lower differential quantum efficiency where an incremental change in current (at high drive current) yields a smaller change in power relative to the response at lower drive currents. This appears as curvature in the current–power curve as shown in Figure 1.11, which can distort the input waveform.

Another important characteristic of directly modulated diode lasers is the rate at which the current can be changed and the corresponding modulation bandwidth. The maximum direct modulation frequency is related to the relaxation-oscillation frequency of the laser cavity. The relaxation-oscillation frequency can be derived from the laser rate equations and is a characteristic frequency that is determined by the interrelationship between the oscillating field in the laser resonator and the atomic inversion. The relaxation-oscillation frequency for a semiconductor laser was given by Lau and Yariv (1985) as

$$f_{\mathrm{r}} = \frac{1}{2\pi}\sqrt{\frac{Ap_0}{\tau_{\mathrm{p}}}}, \tag{1.6}$$

where A is a gain coefficient, p_0 is the intracavity photon density, and τ_{p} is the photon lifetime. Since p_0 is proportional to the drive current above threshold, the modulation bandwidth of the laser diode increases as the drive current is increased (also see Section 8.1). A limitation of direct modulation laser diodes is the inherent noise properties of the source. The relaxation oscillation peak [Equation (1.6)] must be on the same order or higher as the maximum operating frequency. Therefore, any noise present in the drive current below this frequency can manifest as laser RIN in the output light and then eventually in the RF signal output. Thus, there is a tight coupling between the operational bandwidth of a direct-modulation fiber optic link and laser noise. External modulation offers the option to separate these two metrics (laser noise and modulation bandwidth) and thus to optimize each separately.

In external modulation, a continuous wave (CW) laser is modulated by a separate modulator. These devices can take many forms including intensity, phase, or polarization modulators. As mentioned previously,

external modulation allows the laser noise to be optimized independent of the operational bandwidth of the link. A common technique to impress the microwave signal onto a CW laser (E/O conversion) makes use of the electro-optic effect (Kaminow and Turner 1966). The electro-optic effect is a change in the index of refraction of a material due to a change in the applied electric field. This effect is available within certain crystals and is dependent on crystal orientation as described by the crystal's electro-optic coefficients. One common material used in fiber optic links is lithium niobate ($LiNbO_3$), although gallium arsenide, lithium tantalate, and many different organic polymers have also been employed. Figure 1.12 depicts a cross-section of a $LiNbO_3$ modulator. A bulk $LiNbO_3$ substrate is oriented as z-cut, meaning that the z-axis of the crystal is aligned with the primary lines of the input electric field of the optical wave. $LiNbO_3$ has a strong electro-optic coefficient along the z-axis (r_{33}) and a slightly weaker coefficient along the x-axis (r_{23} or r_{13}, depending on the orientation of the coordinate system). Titanium can be diffused into the $LiNbO_3$ substrate to form optical waveguides. After depositing a buffer layer of SiO_2, metal electrodes can then be patterned to form an RF waveguide. Figure 1.12 depicts a coplanar waveguide (CPW) ground-signal-ground (GSG) microwave waveguide where two optical waveguides are diffused below the signal waveguide and one of the ground waveguides. This allows for the applied RF energy to interact (via the electric field lines between the signal-ground electrodes) with the propagating optical signal. The applied RF signal then modifies the index of refraction of the optical waveguide and therefore the phase of the light traveling down the waveguide. In this particular design,

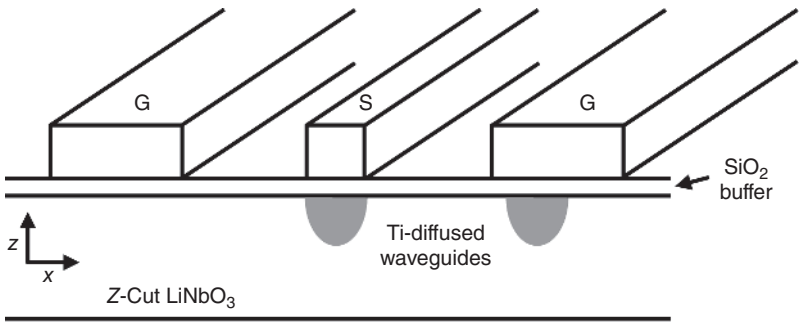

Figure 1.12. Cross-sectional depiction of a z-cut $LiNbO_3$ electro-optic modulator. Metallic ground-signal-ground (GSG) electrodes are patterned over two titanium-diffused optical waveguides.

the optical phase shift in the waveguide under the signal electrode is changed approximately twice as much and with the opposite sign as the phase shift under the ground electrode. Much research has been devoted to the exact construction of these modulators to improve the overlap between the RF fields and optical waveguides (Gopalakrishnan et al. 1992). It is particularly important to ensure that the optical and RF waves travel with the same group velocity and that the transfer of energy from the RF to optical fields is achieved with peak efficiency (Haga et al. 1986). Such "velocity matching" can be quite challenging because of the large difference between the RF and optical indices of refraction for $LiNbO_3$.

The previous discussion illustrates how a microwave signal can interact to change the phase of an optical field within an electro-optic crystal. This is sufficient for creating optical phase modulators, but many optical links use intensity modulation to enable simple demodulation with a photodiode. To convert optical phase modulation into intensity modulation, an optical interferometer is often employed. A common interferometer architecture is the Mach–Zehnder configuration. Figure 1.13(a) shows a basic functional diagram of a Mach–Zehnder modulator (MZM). An optical input is split evenly into two waveguides. The two optical fields are brought together to interfere after some length of propagation. In this example, the two interfering signals are coupled into outputs 1 and 2. Depending on the phase difference between the optical fields, $(\phi_1 - \phi_2)$, the light can constructively or destructively interfere. Figure 1.13(b) shows the intensity at the two optical outputs as a function of the phase difference $(\phi_1 - \phi_2)$. Note how the output intensities are complementary. An intensity modulator can be constructed from this interferometer by phase modulating the fields in either waveguide. Figure 1.13(a) shows an RF CPW over just one of the interferometer waveguides, but in practice, the two optical waveguides can be made very close together as in Figure 1.12. The second waveguide can be patterned directly under the inner ground electrode to increase the RF-to-optical conversion efficiency due to the push–pull nature of the phase shift between the two optical waveguides. Intensity modulation is therefore possible by adjusting the static phase bias $(\phi_1 - \phi_2)$ somewhere along this transfer function, applying an RF input voltage to phase modulate the light and allowing the interferometer to convert this phase modulation into an intensity modulation. Intensity modulation of output I_1 is shown in Figure 1.13(b), but a complementary (180° phase shift) intensity modulation occurs on output I_2. This is useful in the cancellation of

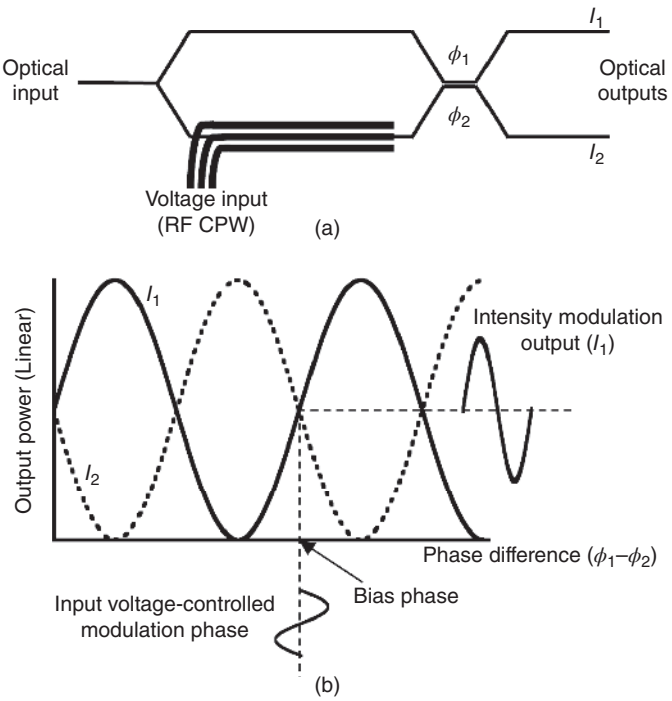

Figure 1.13. (a) Basic Mach-Zehnder modulator (MZM) structure. The RF coplanar waveguide overlaps with a single optical waveguide, but in practice, one ground electrode is patterned over the second optical waveguide as in Figure 1.12. (b) Typical transfer characteristics of an MZM with complementary optical outputs. The modulator is biased with a fixed DC voltage, and an RF signal modulates the lightwave.

some types of optical amplitude noise as demonstrated in Chapter 6. Many other external modulators including Franz–Keldysh semiconductor absorption modulators (Leeson et al. 1988), polarization modulators (Ranalli and Sonek 1991), and modulators based on the index change due to free carrier effects in silicon (Liu et al. 2005) have been demonstrated. Modulators will be discussed in more detail in Chapters 6–8.

Many passive optical components can be used between the E/O and O/E conversions shown as the "processing" block in Figure 1.1. Such components include optical splitters, directional couplers, filters, resonators, attenuators, isolators, circulators, polarizers, and switches. Kashima (1995) provides an extensive description of such optical components. A few devices are described in this chapter. The first is the fused-tapered fiber optic coupler illustrated in Figure 1.14. The fused-tapered fiber optic coupler was proposed by Villarruel and

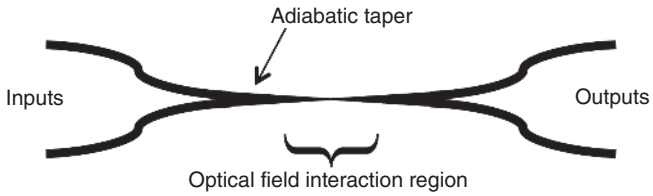

Figure 1.14. Depiction of a 2 × 2 fused-tapered fiber optic coupler.

Moeller (1981) and is a critical component for many systems. The device operates on the concept of electric field resonant coupling between two propagating waveguide modes where the optical evanescent field profiles of the two modes overlap in space. To accomplish this, the waveguide modes must be sufficiently close to one another, as the evanescent fields penetrate only a few micrometers into the cladding of the optical fiber. Therefore, the fibers must be adiabatically tapered to allow the fundamental modes of the fiber to expand into air-guided modes. As the fibers are reduced in diameter, the core can no longer support a guided mode, and the fundamental mode becomes guided by the surrounding air. This allows the electric field of each guided mode to interact, coupling energy from each waveguide into the other. The coupling ratio can be varied if the length over which this field interacts is controlled. This same electric field coupling effect can be used as the output coupler in the interferometric modulator of Figure 1.13(a).

Most passive devices are reciprocal, meaning that their transfer functions are the same in both directions. The fiber optic coupler shown in Figure 1.14 is a common example of a reciprocal device. However, optical isolators and circulators are the often-used nonreciprocal devices. An isolator is commonly employed in laser packages to prevent light backscatter into the laser cavity, which can lead to instabilities. Many lasers, such as DFB lasers, are sensitive to reflections re-entering the cavity (Tkach and Chraplyvy 1986). Most nonreciprocal devices rely on the Faraday Effect, where the polarization state of light is rotated an amount that is proportional to the magnetic field component in the direction of propagation. An optical isolator can be made by inserting a 45° Faraday polarization rotator between two linear polarizers rotated relative to one another by 45°. An incident linear polarization is passed by one polarizer, has its polarization rotated by 45° by the Faraday rotator, and is aligned to pass through the second polarizer. A signal entering from the reverse direction that passes through the output polarizer has its polarization rotated 45° in the opposite direction and impinges on the input polarizer at 90° relative to the transmission polarizer and is

blocked. If two polarizing beamsplitters are combined to handle both linear polarization states, the device can be made to be polarization independent (Chang and Sorin 1990). If a polarizing beamsplitter is added between one of the polarizers and the Faraday rotator, backwards travelling light that would be normally be attenuated by the isolating polarizer could be redirected and coupled out into another fiber resulting in a three-port device that acts as a circulator. Such an optical circulator has the operation characteristics depicted in Figure 1.15. Three low loss transmission states occur as well as three high loss (isolation) paths. Circulators are often used to collect reflections from other devices. For example, they can be used to turn reflective-based optical filters into spectrum separating or combining devices such as wavelength division demultiplexers/multiplexers.

Active devices are also important and are often used in the "processing" block of Figure 1.1. One of the most widely used active components is an optical amplifier. Amplifiers are used to overcome signal attenuation such as from propagation loss, excess loss in components, and loss due to splitting or distribution. Optical amplifiers come in many forms including semiconductor (O'Mahony, 1988), Brillouin (Tkach and Chraplyvy 1989), Raman (Rottwitt and Stentz 2002), and rare-earth-doped fiber amplifiers (Poole et al. 1986). Each has its own advantages and disadvantages (see Sections 3.5 and 4.3); however, the rare-earth-doped fiber amplifier has been the most widely used. In such amplifiers, the core of an optical fiber is doped with a small number of rare-earth ions, Er^{3+} in the case of an EDFA. A basic EDFA design is shown in Figure 1.16. Wavelengths of 980 and 1480 nm have strong absorption cross-sections in Er^{3+} and can therefore be employed as pumps for erbium-doped fiber. This pump light can be combined with a 1550-nm signal into the same fiber using a wavelength division multiplexer (WDM). With the medium inverted, the 1550-nm input light can

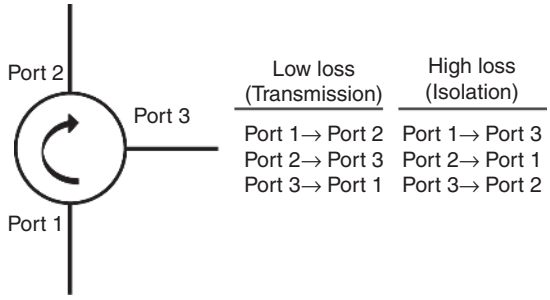

Figure 1.15. Functional diagram of a three-port circulator.

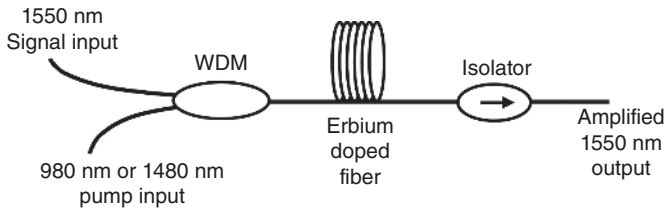

Figure 1.16. Basic components of an erbium-doped fiber amplifier (EDFA).

stimulate the transition of excited erbium ions to their ground states, leading to stimulated emission of photons and thus coherent optical gain. An optical isolator on the output can be employed to prevent reflected light from re-entering the active fiber, which can produce instabilities. Two of the most important properties of the EDFA that make it an ideal amplifier are the low spontaneous emission factor (low noise figure) and the long (milliseconds) upper-state lifetime. The millisecond lifetime does not permit rapid gain fluctuations, and therefore, the signal distortion on high frequency signals ($\gg$kilohertz) is minimal (see Chapter 4). Quantifying the noise performance of an EDFA within an analog link will be covered in Chapter 3.

At the distal end of the link, an O/E converter is required to return the optical signal back into an electric signal. This is most often accomplished with a photodetector. One particular and quite popular photodetector, the p–i–n photodiode, has been used in various forms. Basic architectures include surface-illuminated, waveguide, or travelling-wave designs. The basic structure of a p–i–n photodiode is shown in Figure 1.17, and its performance has been studied extensively. A good review of p–i–n photodiodes is provided by Bowers and Burrus (1987). An intrinsic (undoped) semiconductor is placed between doped p- and n-type materials. The particular materials can be the same (homojunction) or different (heterojunction) and in some special cases do not need to be latticed matched (Ejeckam et al. 1995). A bias voltage is applied to deplete the intrinsic region forming a small parallel-plate capacitor, with higher voltages resulting in a wider depletion region and lower device capacitance. Light can then be absorbed in the intrinsic region by illumination through the p- or n-type materials (surface-illuminated style) or from the edge (waveguide style) creating electron–hole pairs. The photogenerated carriers transit the depletion region and cause image currents to flow in the external circuit. Since the absorption of a photon results in the flow of current, the photodetector acts similarly to a square-law device where it responds only to

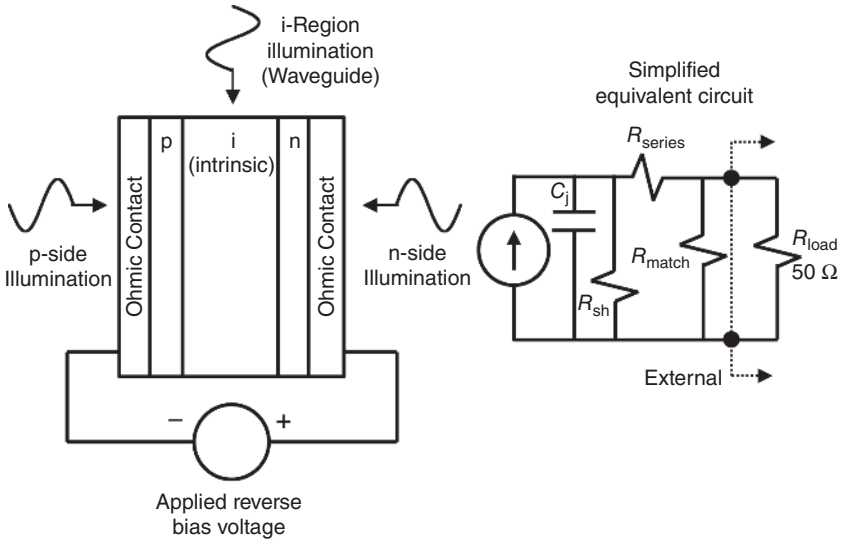

Figure 1.17. A p–i–n photodiode and an equivalent electrical circuit. The photodiode can be surface illuminated either through the n- or p-contacts or parallel to the intrinsic region as would be the case in waveguide architectures.

the optical intensity, thus emitting the optical intensity modulation envelope (the RF input signal) in the form of an output current. The response of these devices is specified in terms of their responsivity in units of Amperes per Watt, how many Amperes of current they produce for every Watt of incident power. Electrically, photodiodes have very simple equivalent circuits if packaging-related impedances are neglected. A photodiode can be viewed as a current source in parallel with a junction capacitance (C_j) and a shunt resistance (R_{sh}), connected to the output through a small series resistance (R_{series}). The junction capacitance is determined by the specific material properties and the geometry, such as the volume of the depletion region. The series resistance is related to the contact resistance and the resistance of the bulk p- and n-type semiconductors. The shunt resistance arises from current leakage and is usually quite high (1 kΩ or more) relative to the RF characteristic impedance of 50 Ω. Therefore, the shunt resistance is usually neglected in photodiode analysis. Since the shunt resistance is usually large, an external matching resistance (R_{match}) is often added to provide a good RF match to the load. This matching resistor has the deleterious effect of shunting half of the photogenerated current and will thus lower link gain by 6 dB. Further details of photodiodes, including other photodiode types, will be discussed in Chapters 4 and 9.

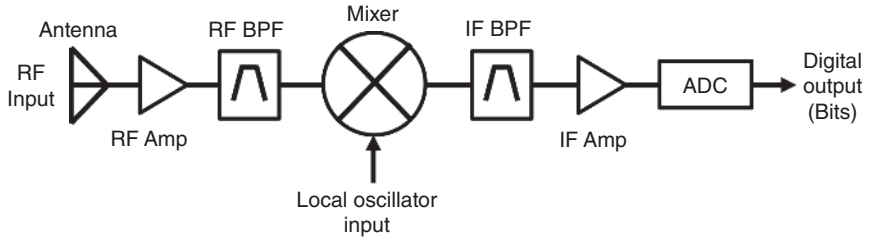

Figure 1.18. Block diagram and typical components contained within an RF receiver.

1.4 ANALOG LINKS WITHIN RF SYSTEMS

Consider the block diagram of a typical RF receiver as shown in Figure 1.18. The goal of such an architecture may be to digitize received RF signals in order to determine the RF situational environment. An antenna receives RF signals from the environment, and those signals are amplified and band limited with a bandpass filter. Since the ADC operates only over a specific bandwidth, a mixer is used to convert the center frequency of the RF signal to that of the ADC. After frequency conversion, the signal is filtered and amplified to a level within the dynamic range of the ADC, which has n bits of resolution at a given sampling rate.

There are numerous advantages of applying RF photonics to the architecture shown in Figure 1.18. For example, a fiber optic link can be inserted between the antenna and the input RF amplifier or between the input RF amplifier and the electronic mixer in order to remote the back end from the front end. In this case, a system trade space analysis considering loss (see Figure 1.7), noise figure, and dynamic range is appropriate. If a multichannel antenna system is required, as in direction-finding applications, phase stability might also be considered in the analysis. A fiber optic solution affords improved phase stability over all-electronic approaches (see Figure 1.8). If the noise figure performance of a photonic link is acceptable, the post-antenna amplifier can potentially be removed. Removing this amplifier can help to reduce distortion because low noise RF amplifiers can exhibit relatively small dynamic range. Photonic channelization with resolution approaching what is required in the electronic domain is becoming a realization; thus, the filter in Figure 1.18 might be replaced with an optical equivalent. Other real possibilities for the injection of photonics in such a system include optical down conversion and optical ADC. The possibilities are

limited only by the ingenuity of the system designer and the available photonic technologies.

This book entails a fundamental approach to the description and analysis of microwave photonics technology. The work begins with basic principles as a foundation in Chapters 2 through 5. An analysis of numerous link architectures follows in Chapters 6 through 8. Chapter 9 deals with the design and performance of high current photodetectors. The last chapter focuses on specific applications and system-level considerations for microwave photonics. The text presented in this book provides a thorough treatment of the field—hopefully one that will provide a spark for insightful scientists and engineers to innovate new photonic solutions at the RF system level.

REFERENCES

Berceli, T. and Herczfeld, P. R., "Microwave photonics—a historical perspective," *IEEE Trans. on Microwave Theory and Techniques*, 58(11), 2992–3000 (2010).

Bowers, J. E., Burrus, C. A., and McCoy, R. J., "InGaAs PIN photodetectors with modulation response to millimetre wavelengths," *Electronics Letters*, 21(18), 812–814 (1985).

Bowers, J. E., and Burrus, C. A., "Ultrawide-band long-wavelength p-i-n photodetectors," *Journal of Lightwave Technology*, 5(10), 1339–1350 (1987).

Campillo, A., Tulchinsky, D., Funk, E., and Williams, K., "RF phase distortion due to crosstalk in an 8 channel wavelength division multiplexed analog delay line," *Optical Fiber Communications Conference* 2003 729–730 (2003).

Chang, K. W. and Sorin, W. V., "High-performance single-mode fiber polarization-independent isolators," *Optics Letters*, 15(8), 449–451 (1990).

Chiddix, J. A., Laor, H., Pangrac, D. M., Williamson, L. D., and Wolfe, R. W., "AM video on fiber in CATV systems: need and implementation," *IEEE Journal on Selected Areas in Communications*, 8(7), 1229–1239 (1990).

Ejeckam, F. E., Chua, C. L., Zhu, Z. H., Lo, Y. H., Hong, M., and Bhat, R., "High-performance InGaAs photodetectors on Si and GaAs substrates," *Applied Physics Letters*, 67(26), 3936–3938 (1995).

Essiambre, R. J., Kramer, G., Winzer, P. J., Foschini, G. J., and Goebel, B., "Capacity limits of optical fiber networks," *Journal of Lightwave Technology*, 28(4), 662–701 (2010).

Essiambre, R. J., Tkach, R. W., and Ryf, R., "Fiber nonlinearity and capacity: single-mode and multimode fibers," in *Optical Fiber Telecommunications VIB*, Academic (2013).

French, W. G., MacChesney, J. B., O'Connor, P. B., and Tasker, G. W., "Optical waveguides with very low losses," *Bell System Technology Journal*, 53(5), 951–954 (1974).

Fuller, K. L., "To see and not be seen," *IEE Proceedings F, Radar and Signal Processing*, 137(1), 1–10 (1990).

Gopalakrishnan, G. K., Bulmer, C. H., Burns, W. K., McElhanon, R. W., and Greenblatt, A. S., "40 GHz, low half-wave voltage Ti:LiNbO3 intensity modulator," *Electronics Letters*, 28(9), 826–827 (1992).

Haga, H., Izutsu, M., and Sueta, T., "$LiNbO_3$ traveling-wave light modulator/switch with an etched groove," *IEEE Journal of Quantum Electronics*, 22(6), 902–906 (1986).

Hartog, A. H., Conduit, A. J., and Payne, D. N., "Variation of pulse delay with stress and temperature in jacketed and unjacketed optical fibers," *Optical and Quantum Electronics*, 11(3), 265–273 (1979).

Horiguchi, M., and Osanai, H., "Spectral losses of low-OH content optical fibers," *Electronics Letters*, 12(12), 310–312 (1976).

Kaiser, P., Tynes, A. R., Astle, H. W., Pearson, A. D., French, W. G., Jaeger, R. E., and Cherin, A. H., "Spectral losses of unclad vitreous silica and soda-lime-silicate fibers," *Journal of the Optical Society of America*, 63(9), 1141 (1973).

Kaminow, I. P. and Turner, E. H., "Electrooptic light modulators," *Applied Optics*, 5(10), 1612–1628 (1966).

Kapron, F. P., "Radiation losses in glass optical waveguides," *Applied Physics Letters*, 17(10), 423–425 (1970).

Kashima, N., *Passive Optical Components for Optical Fiber Transmission*, Boston: Artech House, USA (1995).

Kawachi, M., Kawana, A., and Miyashita, T., "Low-Loss Single-Mode Fiber at Material Dispersion-Free Wavelength of 1.27 μm," *Electronics Letters*, 13(15), 442–443 (1977).

Khilo, A., et al., "Photonic ADC: overcoming the bottleneck of electronic jitter," *Optics Express*, 20(4), 4454–4469 (2012).

Lau, K. Y. and Yariv, A., "Ultra-high speed semiconductor lasers," *IEEE Journal of Quantum Electronics*, 21(2), 121–138 (1985).

Leeson, M. S., Payne, F. P., Mears, R. J., Carroll, J. E., Roberts, J. S., Pate, M. A., and Hill, G., "Design and fabrication of a planar, resonant Franz-Keldysh optical modulator," *IEE Colloquium on Optics in Computing*, 8 (1988).

Liebe, H. J., "Atmospheric EHF Window Transparencies near 35, 90, 140, and 220 GHz," *IEEE Transactions on Antennas and Propagation*, AP-31(1), 127–135 (1983).

Liu, A., Samara-Rubio, D., Liao, L., and Paniccia, M., "Scaling the modulation bandwidth and phase efficiency of a silicon optical modulator," *IEEE Journal of Selected Topics in Quantum Electronics*, 11(2), 367–372 (2005).

Lockman, F. J., "The Green Bank Telescope: an overview," *Proceedings of SPIE*, 3357, 656–665 (1998).

Mecozzi, A., and Essiambre, R., "Nonlinear Shannon Limit in Pseudolinear Coherent Systems," *Journal of Lightwave Technology*, 30(12), 2011–2024 (2012).

Morton, P. A., Logan, R. A., Tanbun-Ek, T., Sciortino Jr., P. F., Sergent, A. M., Montgomery, R. K., and Lee, B. T., "25 GHz bandwidth 1.55 μm GaInAsP p-doped strained multiquantum-well lasers," *Electronics Letters*, 28(23), 2156–2157 (1992).

Murata, H., and Inagaki, N., "Low-loss single-mode fiber development and splicing research in Japan," *IEEE Journal of Quantum Electronics*, 17(6), 835–849 (1981).

Nagarajan, R., Ishikawa, M., Fukushima, T., Geels, R. S., and Bowers, J. E., "High speed quantum-well lasers and carrier transport effects," *IEEE Journal of Quantum Electronics*, 28(10), 1990–2008 (1992).

Nakazawa, M., "Ultrahigh spectral density coherent optical transmission techniques," in *High Spectral Density Optical Communications Technologies*, M. Nakazawa, K. Kikuchi and T. Miyazaki (editors), pp. 51–80, Springer (2010).

Nazarathy, M., Berger, J., Ley, A. J., Levi, I. M., and Kagan, Y., "Progress in externally modulated AM CATV transmission systems," *Journal of Lightwave Technology*, 11(1), 82–105 (1993).

Norman, R. F. and Meullen, N. F., "Towed Target," US Patent 3,135,511, 2 1964.

Nyquist, H., "Certain Topics in Telegraph Transmission Theory," *Transactions of the American Institute of Electrical Engineers*, 47(2), 617–644 (1928).

Okamoto, H. "Semiconductor Quantum-Well Structures for Optoelectronics–Recent Advances and Future Prospects," *Japanese Journal of Applied Physics*, 26(Part 1, No. 3), 315–330 (1987).

Okamoto, S., Toyoda, K., Omiya, T., Kasai, K., Yoshida, M., and Nakazawa, M., "512 QAM (54 Gbit/s) coherent optical transmission over 150 km with and optical bandwidth of 4.1 GHz," in *European Conf. on Optical Communications*, 1–3 (2010).

Olshansky, R., Powazinik, W., Hill, P., and Lanzisera, V., "InGaAsP buried heterostructure laser with 22 GHz bandwidth and high modulation efficiency," *Electronics Letters*, 23(16), 839–841 (1987).

O'Mahony, M. J., "Semiconductor laser optical amplifiers for use in future fiber systems," *Journal of Lightwave Technology*, 6(4), 531–544 (1988).

Page, R. M., "The Early History of Radar," *Proceedings of the IRE*, 50(5), 1232–1236 (1962).

Payne, J. M. and Shillue, W. P., "Photonic techniques for local oscillator generation and distribution in millimeter-wave radio astronomy," *IEEE International Topical Meeting on Microwave Photonics*, MWP 2002, *Paper* W1-3, 9–12 (2002).

Phillips, M. R., and Ott, D. M., "Crosstalk due to optical fiber nonlinearities in WDM CATV lightwave systems," *Journal of Lightwave Technology*, 17(10), 1782–1792 (1999).

Poole, S., Payne, D., Mears, R., Fermann, M., and Laming, R., "Fabrication and characterization of low-loss optical fibers containing rare-earth ions," *Journal of Lightwave Technology*, 4(7), 870–876 (1986).

Prestage, R. M., Constantikes, K. T., Hunter, T. R., Kinig, L. J., Lacasse, R. J., Lockman, F. J., and Norrod, R. D., "The Green Bank Telescope," *Proceedings of the IEEE*, 97(8), 1382–1390 (2009).

Ramo, S., Whinnery, J. R., and Duzer, T. V., *Fields and Waves in Communications Electronics*, p. 413, Wiley, New York (1994).

Ranalli, E. R., and Sonek, G. J., "Narrow bandwidth electrooptic polarization modulator using GaAs quantum-well waveguides," *IEEE Photonics Technology Letters*, 3(4), 320–323 (1991).

Redd, J. and Lyon, C., "Spectral content of NRZ test patterns," *EDN Magazine*, 49(9), 10–14 (2004).

Roman, J., Frankel, M., Williams, K., and Esman, R., "Optical fiber cables for synchronous remoting of numerous transmitters/receivers," *IEEE Photonics Technology Letters*, 10(4), 591–593 (1998a).

Roman, J. E., Nichols, L. T., Williams, K. J., Esman, R. D., Tavik, G. C., Livingston, M., and Parent, M. G., "Fiber-optic remoting of an ultrahigh dynamic range radar," *IEEE Transactions on Microwave Theory and Techniques*, 46(12), 2317–2323 (1998b).

Rottwitt, K. and Stentz, A. J., "Raman amplification in lightwave communication systems," in *Optical Fiber Telecommunications IVA*, I. Kaminow and T. Li (editors), Academic (2002).

Shannon, C. E., "Communication in the presence of noise," *Proceedings of the IRE*, 37(1), 10–21, (1949).

Su, C., and Lanzisera, V., "Ultra-high-speed modulation of 1.3-μm InGaAsP diode lasers," *IEEE Journal of Quantum Electronics*, 22(9), 1568–1578 (1986).

Takahashi, H., Amin, A. A., Jansen, S. L., Morita, I., and Tanaka, H., "Highly spectrally efficient DWDM transmission at 7.0 b/s/Hz using 8x65.1-Gb/s coherent PDM-OFDM," *Journal of Lightwave Technology*, 28(4), 406–414 (2010).

Testi, L. and Walsh, J., "The inauguration of the Atacama large millimeter/submillimeter array," *The Messenger*, 152, 2–6 (2013).

Thacker, D. L., and Shillue, B., "Atacama large millimeter array local oscillator: how photonics is enabling millimeter-wave astronomy," in *2011 Optical Fiber Communication Conference*, paper OThJ1, (2011).

Tkach, R., and Chraplyvy, A., "Regimes of feedback effects in 1.5-μm distributed feedback lasers," *Journal of Lightwave Technology*, 4(11), 1655–1661 (1986).

Tkach, R. W., and Chraplyvy, A. R., "Fibre Brillouin amplifiers," *Optical and Quantum Electronics*, 21, S105–S112 (1989).

Toman, D. "Towed Decoy with Fiber Optic Link," US Patent 4,808,999, 28 Feb (1989).

Villarruel, C. A. and Moeller, R. P., "Fused single mode fibre access couplers," *Electronics Letters*, 17(6), 243–244 (1981).

Walden, R. H., "Analog-to-digital converter survey and analysis," *IEEE Journal on Selected Areas in Communications*, 17(4), 539–550 (1999).

Walden, R. H., "Analog-to-digital converters and associated IC technologies," in *IEEE Compound Semiconductor Integrated Circuits Symposium*, 1–2 (2008).

Webber, J. C. and Pospieszalski, M. W., "Microwave instrumentation for radio astronomy," *IEEE Transactions on Microwave Theory and Techniques*, 50(3), 986–995 (2002).

Weisser, S., Larkins, E. C., Czotscher, K., Benz, W., Daleiden, J., Esquivias, I., Fleissner, J, Ralston, J. D., Romero, B., J., Sah, R. E., Schonfelder, A., and Rosenzweig, J., "Damping-limited modulation bandwidths up to 40 GHz in undoped short-cavity In0.35Ga0.65As-GaAs multiple-quantum-well lasers," *IEEE Photonics Technology Letters*, 8(5), 608–610 (1996).

White, S. D., "Implementation of a photonic automatic gain control system for correcting gain variations in the Green Bank Telescope fiber optic system," *Review of Scientific Instruments*, 71(8), 3196–3199 (2000).

Wiltse, J. C., "Corrections to published curves for atmospheric attenuation in the 10 to 1000 GHz region," *IEEE Antennas and Propagation Society International Symposium*, 4, 2580–2583 (1997).

Winzer, P. J., Gnauck, A. H., Doerr, C. R., Magarini, M., and Buhl, L. L., "Spectrally Efficient Long-Haul Optical Networking Using 112-Gb/s Polarization-Multiplexed 16-QAM." *Journal of Lightwave Technology*, 28(4), 547–556 (2010).

Zhou, X., Yu, J., Qian, D., Wang, T., Zhang, G., and Magill, P. D., "8x114 Gb/s, 25-GHz-spaced, PolMux-RZ-8PSK transmission over 640 km of SSMF employing digital coherent detection and EFDA-only amplification," in *Optical Fiber Communication Conference*, Post-Deadline Paper PDP1 (2008).

Zhou, X., Yu, J., Huang, M. F., Shao, Y., Wang, T., Magill, P., Cvijetic, M., Nelson, L., Birk, M., Zhang, G., Ten, S., Matthew, H. B., and Mishra, S. K., "Transmission of 32-Tb/s capacity over 580 km using RZ-shaped PDM-8QAM modulation format and cascaded multimodulus blind equalization algorithm," *Journal of Lightwave Technology*, 28(4), 456–465 (2010).